Chemical Engineering Journal 451 (2023) 138709

Contents lists available at ScienceDirect

Chemical Engineering Journal

journal homepage: www.elsevier.com/locate/cej

Kinetic modeling of the hydrocracking of polystyrene blended with vacuum gasoil

David Trueba [a], Roberto Palos [a,b], Javier Bilbao [a], José M. Arandes [a], Alazne Gutiérrez [a,*]

[a] Department of Chemical Engineering, University of the Basque Country UPV/EHU, PO Box 644, 48080 Bilbao, Spain
[b] Department of Chemical and Environmental Engineering, University of the Basque Country UPV/EHU, Plaza Ingeniero Torres Quevedo 1, 48013 Bilbao, Spain

ARTICLE INFO

Keywords:
Hydrocracking
Kinetic modeling
Waste plastics
Polystyrene
Vacuum gasoil
Catalyst deactivation

ABSTRACT

The kinetic modeling of the hydrocracking of a mixture of polystyrene (PS) and vacuum gasoil (VGO) over a PtPd/HY catalyst has been carried out. The reactions have been performed in a batch reactor under the following conditions: 380–420 °C; 80 bar; content of PS in the feed, 10 wt%; catalyst/feed ratio, 0.1 in mass; and time, 30–300 min. Different reaction networks and kinetic models have been studied, in which the evolution of product distribution (unconverted PS, dry gas, liquefied petroleum gases, naphtha, light cycle oil, heavy cycle oil and coke) with the extent of time has been quantified by considering three different simultaneous deactivation mechanisms (plastic fouling, coke deposition and metal poisoning). The kinetic model selected (based on a 7-lump reaction network) has been used for performing a parametric study, determining that 400 °C and 180 min are the optimal conditions for maximizing the yield of naphtha (35 wt%) at the same time that PS is totally converted. This original kinetic model may act as a basis for scaling-up studies focused on the large-scale valorization of waste plastics by co-feeding them into a hydrocracking unit of a Waste-Refinery.

1. Introduction

The growth of plastic demand in the packaging, automotive, construction and electrical and electronics industries does not come with an efficient waste management [1]. Consequently, this waste is mainly landfilled and incinerated provoking different phenomena that interfere with human health [2,3], such as the presence of microplastics in aquifers and oceans and the emission of toxins in uncontrolled incineration. In this context, the thermochemical technologies suitable for treating waste plastics (pyrolysis, gasification, cracking and hydrocracking) [4,5] are attracting attention in recent times since they offer the possibility of recovering monomers and producing fuels or hydrogen. One of the main difficulties when establishing the best valorization route is the heterogeneous character of the waste plastics, whose average distribution in the European Union urban solid wastes is the following [6]: polypropylene (PP), 26 wt%; high density polyethylene (HDPE), 15 wt%; low density polyethylene (LDPE), 13 wt%; linear low density polyethylene (LLDPE), polyvinyl chloride (PVC), 20 wt%; polystyrene (PS), 7 wt%; polyethylene terephthalate (PET), 6 wt%, and; others, 5 wt%. Pyrolysis has revealed itself as a straightforward technology of adequate application for the valorization of waste plastics [7]. For example, waste PET pyrolysis [8] appears to be successful for the production of gases (CO, CO_2, ethylene), along with commercial interest solids (benzoic and benzoyl formic acid) and oil. Apart from that, the technological development of gasification is also remarkable [9].

The possibility of co-feeding waste plastics or their derivatives obtained in a fast pyrolysis stage with benchmark streams to conventional refinery units (Waste-Refinery) has emerged as a promising strategy that can be the solution for the major waste plastics mismanagement (specifically polyolefins) [6] through their conversion into fuel and chemical. In this way, the valorization of waste plastics within the refineries would ease the integration of the oil industry in the circular economy action plan, since the valorization of goods produced with petroleum derivatives would be performed resulting in an oil consumption reduction. The production will be optimized according to the capacity of the refinery units in order to adapt the composition of the products to legal requirements and, subsequently, promote their commercialization and distribution by the conventional distribution channels. The refinery units with a potentially key role within the Waste-Refinery are those of catalytic processing. Thus, the potential of fluid catalytic cracking (FCC) has been explored by feeding HDPE dissolved in vacuum gas oil (VGO) [10] and mixtures of HDPE pyrolysis waxes and VGO [11]. Palos et al.

* Corresponding author.
E-mail address: alazne.gutierrez@ehu.eus (A. Gutiérrez).

https://doi.org/10.1016/j.cej.2022.138709
Received 20 June 2022; Received in revised form 26 July 2022; Accepted 17 August 2022
Available online 22 August 2022

Nomenclature

Abbreviations

DG	dry gas
HCO	heavy cycle oil
LCO	light cycle oil
LPG	liquefied petroleum gases
PS	polystyrene

Symbols

C_c	carbon content deposited on the catalyst, $g_{coke}\ g^{-1}_{catalyst}$
E_j	activation energy of the reaction *j*, kJ/mol
$F_{1-\alpha}$	Fisher's distribution critical value
F_{A-B}	Fisher's test value
$k_{d,c}$	catalyst deactivation rate constant related to coke deposition
$k_{d,m}$	catalyst deactivation rate constant related to metals poisoning
k_j	reaction rate constant of reaction *j*
$k_{j,Tref}$	reaction rate constant of reaction *j* at temperature of reference
M	metal loading of the catalyst, kg of metal (kg of catalyst)$^{-1}$
M_0	maximum metal loading of the catalyst, kg of metal (kg of catalyst)$^{-1}$
m_c	coke deactivation rate order
m_m	metals poisoning rate order
n_d	number of experimental data
n_e	number of experiments
n_l	number of lumps
n_p	number of experimental data
R	universal gas constant, kJ/mol
SSE	sum of square errors
t	reaction time, min
T	temperature of reaction, K
t_b	catalyst pores blockage time, min
T_{ref}	reference temperature, K
W	catalyst mass, g
Y_i	yield of i lump, wt%

Superscripts

n	number of deactivation types
α_j	order of reaction *j*

Subscripts

A, B	compared models
c	coke deactivation
i	certain lump
j	certain reaction
k	certain type of deactivation
m	deactivation by metals poisoning
p	deactivation by PS deposition
s	steady state

Greek symbols

α	deactivation constant of coke deposition
φ	activity function
ψ	global activity
υ	degrees of freedom

[12] have developed a kinetic model for HDPE waxes cracking.

Regarding waste plastics hydroprocessing, it has been studied principally with virgin plastics [13], aiming to maximize transport fuel production [14]. Vance et al. [15] have studied polyethylene hydrocracking with a catalyst and under specific operating conditions that promote the isomerization obtaining isoparaffinic gasoline as the main product, while Choi et al. [16] have studied the hydrocracking of pyrolysis waxes. The attractiveness of the hydroprocessing refinery units to add value to the waste plastics or their pyrolysis waxes lies in their versatility for treating heavy and aromatic streams, obtaining products with a composition similar to that of commercial fuels by using the appropriate operating conditions and catalysts [17]. Vela et al. [18,19] have checked that the co-feeding of HDPE with VGO has the interest of increasing the conversion of the VGO and reducing the concentration of aromatics in the naphtha fraction produced. The same authors [19] have compared the results of the different strategies of co-feeding HDPE or plastic pyrolysis oil (PPO) with VGO. However, making the upgrading of waste plastics in refinery hydroprocessing units come true it is required the knowledge of kinetic models that would allow for (i) predicting the effects of the operating conditions in the product distribution, (ii) optimizing the operating conditions and (iii) defining the possible revamping requirements of the units.

The kinetic modeling of catalytic processes such as cracking and hydrocracking of hydrocarbons (which present a complex reaction network) shows particular difficulties predicting the evolution over time of the product distribution due to deactivation. Consequently, well-established software such as Advances Kinetics and Technology Solutions (AKTS) cannot be used as it is in the cases of thermokinetic results of waste plastics pyrolysis [20]. The fundaments for the kinetic modeling of the hydroprocessing of heavy refinery streams have been developed by means of studies carried out in batch reactors with slurry-phase catalysts [21]. The kinetic models that consider the reactions of the individual components [17] require a bigger experimental base and a calculation methodology far more complex than the lump-based models [22]. These models composed of discrete lumps are simpler and allow for more easily quantifying phenomena that, given their complexity, are normally empirically quantified, such as the diffusional limitations of the components in the reaction media and the deactivation of the catalysts [23]. The lumps are groups of compounds with similar kinetic behavior that are treated as pseudo-components in the modeling. In the hydroprocessing of heavy petroleum fractions, the lumps are established according to: (i) boiling point criteria basis into dry gas (DG), liquefied petroleum gases (LPG), naphtha, light cycle oil (LCO), heavy cycle oil and coke (carbon deposited on the catalyst), using different strategies for establishing the appropriate reaction network [24], performing sensibility analyses to simplify the models [25], and relating kinetic parameters values with those in the literature [26]; or (ii) SARA (saturates, aromatics, resins and asphaltenes) composition [27,28], using separate models to predict liquid, gas and coke yields [29].

The modeling of the hydrocracking of VGO has been carried out using kinetic models with between 4 and 9 component lumps [24,30]. In contrast, the precedent works in the literature about the kinetic modeling of the hydrocracking of plastics are very scarce. Bin Jumah et al. [28] proposed for the hydrocracking of light-density polyethylene (LDPE) over a Pt/Hbeta catalyst a 4-lump (LDPE, heavy liquids, naphtha and gases) scheme of reactions. They obtained that the limiting step was the conversion of the LDPE into heavy liquid, given the diffusional restrictions that the macromolecular chains of LDPE encountered within the structure of the zeolite.

In a previous work [31], we investigated the co-feeding of polystyrene (PS) and VGO under different operating conditions (temperature and reaction time) in a semi-batch reactor using a PtPd/HY catalyst. Indeed, an exhaustive characterization of the deactivated catalysts was also carried out to deeply understand the deactivation phenomena involved in the hydrocracking of PS/VGO blend and its consideration for

kinetic modeling. The aromatic nature of PS requires (just like VGO) hydrocracking in order to maximize naphtha production with the adequate composition for its commercialization as gasoline. In this work, the data obtained in those experiments have been used to establish an innovative lump-based kinetic model. In addition, each deactivation mechanism has been modeled using each own equation, in order to predict the evolution of the product distribution. Thus, four different models have been tested and the election of the optimal one has been made by statistical methods. Finally, the best kinetic model has been used to find the optimal operating conditions to maximize the conversion of PS and the production of naphtha, which can be assimilated by commercial gasoline. The interest of the kinetic model lies on its application to the hydrocracking unit and the proposed methodology will be used as basis for the study of the hydrocracking with different plastics and catalysts.

2. Materials and methods

2.1. Charges

The vacuum gasoil (VGO) has been provided by Petronor refinery (Muskiz, Spain). The techniques used for its characterization have been already detailed in a previous work [31]. The main physicochemical properties of the VGO can be found in Table S1 in the Supplementary Material. In short, it consists of a mix of hydrocarbons, mainly paraffins (49 wt%) and with a remarkable content of 3^+-ring aromatics (24.5 wt %), with a boiling range (408–503 °C) that corresponds to a light VGO.

The polystyrene (PS) has been purchased from Dow Chemical in Tarragona (Spain). It has been received in 4 mm pellet form and prior to being blended with the VGO it has been milled to dust by cryogenic methods. The main properties of the PS (molecular weight, 311.6 kg mol^{-1}; density, 1.030 g mL^{-1}; and dispersity, 2.39) have been provided by the supplier.

2.2. Catalyst

A PtPd catalyst supported on a Y zeolite has been used for the hydrocracking runs. The nominal content for each metal is 0.5 wt%. The synthesis procedure, as well as the characterization techniques used can be found in a previous work [31]. Shortly, the textural properties have been obtained through N_2 adsorption–desorption isotherms; the acidic properties have been measured by means of ammonia temperature-programmed desorption (TPD) and pyridine Fourier-transform infrared spectroscopy (FTIR) spectra; the actual metal content has been quantified by inductively coupled plasma-optical emission spectrometry (ICP-OES); and metal dispersion has been calculated by CO pulse chemisorption. From the properties (Table S2), it should be highlighted the relatively high specific surface area (548 $m^2\ g^{-1}$), which is a consequence of the contribution of the micropores surface (368 $m^2\ g^{-1}$). Moreover, it has a total acidity of 0.465 $mmol_{NH3}\ g^{-1}$and a Brønsted/Lewis (B/L) ratio of 0.98. Finally, it should be remarked the dispersion of the metals on the support (47.8 %).

2.3. Reaction equipment and procedure

The hydrocracking runs have been carried out in an already described experimental setup [32], which consists of a 50 mL batch reactor that operates in semi-continuous regime and under the following operating conditions: 380–420 °C, 80 bar, 30–300 min and with catalyst-to-feed and plastic-to-feed ratios of 0.1 in mass basis in both cases. The stirring speed of the reactor has been established at 1300 rpm in order to minimize the external diffusion limitations. Note that the stirring has been switched on once the established temperature and pressure conditions have been reached, considering that very moment the zero time of reaction. The experimental setup is also equipped with a condensation system that ensures the proper separation of the light volatile species. Furthermore, prior to the reaction, the catalyst has been reduced to achieve its active form. The reduction has been carried out *ex-situ* in a fixed bed reactor at 400 °C for 4 h under a mixture of gases consisting of a 30 mL min^{-1} flow of H_2 and a 50 mL min^{-1} flow of N_2.

2.4. Analysis of products

The products have been submitted to different analyses in order to properly characterize them. But, first of all, it should be detailed which has been the procedure followed for differentiating them, i.e. for properly closing the mass balance. The amount of gas has been obtained as the difference between the weight of the reactor before and after the reaction. For determining the amount of non-converted plastic a procedure composed of two consecutive extractions has been required (Fig. S1). The amount of coke deposited on the spent catalysts has been quantified by means of temperature-programmed oxidation (TPO). Finally, the amount of liquid products has been obtained as the difference between the mass of the feedstock loaded into the reactor and the mass of the other products obtained according to the aforementioned calculations.

The gas products have been analyzed by gas chromatography in an Agilent Technologies 6890 GC equipped with an HP-PONA capillary column (50 m × 0.2 mm) and an FID detector. For properly separating the lightest hydrocarbons, the analysis has been carried out at cryogenic temperatures (-30 °C) using CO_2 for reaching that temperature. The gas fraction has been separated into dry gas (DG, C_1-C_2) and liquefied petroleum gases (LPG, C_3-C_4).

The liquid products have been divided into three different lumps according to the following boiling ranges (T_B): naphtha (T_B less than 216 °C), light cycle oil (LCO, 216 < T_B < 343 °C) and heavy cycle oil (HCO, T_B greater than 343 °C). For performing this differentiation, the liquid products have been submitted to a simulated distillation analysis according to the procedure specified in the ASTM D2887 Standard. Likewise, they have been analyzed in an Agilent Technologies 6890 gas chromatograph equipped with a DB-2887 semi-capillary column (10 m × 0.53 mm) and an FID detector.

The methodology used has allowed to quantify the total amount of coke as well as to distinguish between the coke located on the external surface of the catalyst and that deposited within the pore system of the zeolite [33]. Apart from that, scanning electron microscopy (SEM) images of the spent catalysts have been recorded to ratify which is the predominant deactivation phenomenon at each temperature. The apparatus used has been a Schottky-type field emission scanning electron microscope (JEOL JSM-7000F) equipped with a secondary electron detector working at 10 kV. Finally, the content of metals on the spent catalysts has been also measured by ICP-OES analysis in an Agilent Technologies 7200-ES equipment, after submitting the samples to digestion in an HNO_3, HCl and HF mixture.

3. Kinetic modeling

To the best of our knowledge, there are no other kinetic studies about the hydrocracking of PS/VGO blends. Therefore, the different models proposed for the hydrocracking of heavy oil [34] have been taken as the starting point.

3.1. Reaction network

The discrimination of the different kinetic models has been focused on the two reaction networks collected in Fig. 1. Model A (Fig. 1a) consists of a 6-lump reaction network, quite similar to that proposed by Martínez and Ancheyta [34] for the hydrocracking of heavy oil, to which the PS has been added. As it can be seen, the network considers a parallel-series system of reactions in which the hydrocracking of the heavy species into lighter ones occurs sequentially. In addition, it has been considered that just the compounds within the HCO lump could

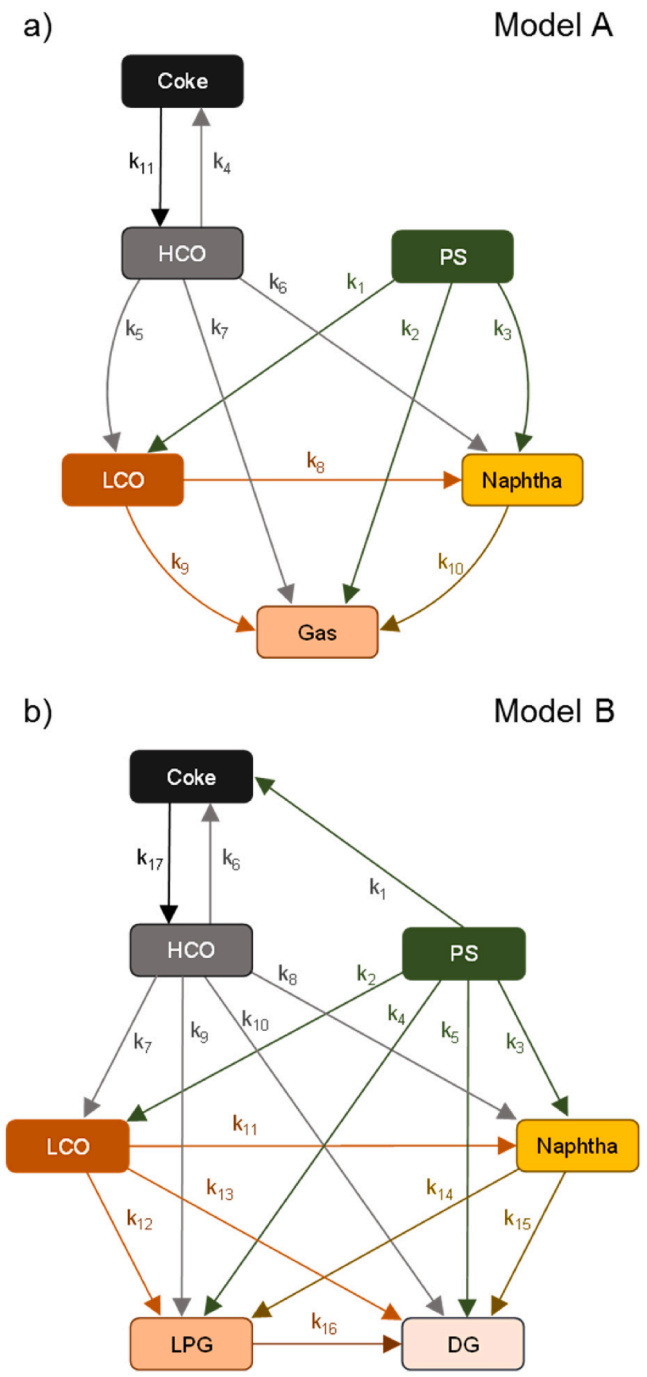

Fig. 1. Proposed 6-lump (model A) (a) and 7-lump (model B) (b) reaction networks.

condensate forming coke. However, some coke precursors can be also hydrogenated making this reaction a two-way pathway. Hence, the reactions in model A account for a total amount of 11 kinetic constants. The second proposal (model B in Fig. 1b), more complex, splits the gas lump into DG and LPG lumps, becoming a 7-lump reaction network. Additionally, it has been also considered the formation of coke from the PS, without taking into account the inverse route. The enlargement of the reactions system adds 6 new kinetic constants (accounting for a total amount of 17 in model B), 5 corresponding to the formation of dry gas from the rest of the lumps and the remaining one corresponding to the polystyrene-to-coke pathway.

3.2. Mass conservation equations

The methodology used for the kinetic data analysis is in concordance with the stages and the recommendations established in the literature for catalytic processes with complex reaction networks that consider the catalyst deactivation [35]. Furthermore, to establish the mass conservation equations of the different lumps, the following assumptions have been made: (i) external diffusivity is negligible due to the stirring speed used in the experiments [27]; (ii) gas and liquid phase concentrations are uniform in the reactor; (iii) a high heat transmission is achieved avoiding the formation of temperature gradients in the reactor [36], considering the reactor as isothermal; (iv) the continuous feeding of H_2 creates an excess of this reactant that allows considering that pressure is constant within the reaction medium over time; and (v) the catalyst deactivation is due to three simultaneous causes, namely plastic fouling, coke deposition and metal poisoning (as explained in Section 3.3).

This way, the evolution over time of the yield of each lump *i* within the reaction network (Y_i) is represented by the following conservation equation:

$$\frac{dY_i}{dt} = \psi \sum_{1}^{j} k_j (Y_i)^{n_j} \quad (1)$$

where k_j is the kinetic parameter, n_j is the order of reaction *j* and ψ is the global deactivation function, considering that the effect of deactivation in the individual reaction kinetics is non-selective. In concordance with the common treatment in the literature [37], the individual reactions have been considered of first order ($n_j = 1$) except for those in which the HCO lump (heavy fraction of the VGO) is involved, which are of second order ($n_j = 2$).

In order to express the temperature dependence of the kinetic parameters, they have been defined according to the reparameterized Arrhenius equation [38].

$$k_j = k_{j,Tref} \exp\left[-\frac{E_j}{R}\left(\frac{1}{T} - \frac{1}{T_{ref}}\right)\right] \quad (2)$$

being $k_{j,Tref}$ the kinetic parameter of reaction *j* at the reference temperature, E_j the activation energy of reaction *j*, R the universal gas constant, T the temperature and T_{ref} the reference temperature (673 K).

3.3. Deactivation causes and kinetics

The rigorous quantification of the deactivation is one of the main challenges of the kinetic modeling of the hydrocracking of heavy oil fractions. However, this goal faces the difficulty of establishing the kinetic models of various simultaneous causes. In hydrocracking reactions, the principal deactivation causes are the formation of coke (carbonaceous material that covers sequentially the active sites and micropores of the acid support) and the poisoning of the metallic sites caused by the presence of metals in the feed [23]. As an illustrative example of pore blockage, nitrogen adsorption–desorption isotherms of spent catalysts at the intermediate temperature have been collected in Fig. S2, observing both a general decrease in the surface properties of the fresh catalyst that evidences the blockage on *meso-* and micro-pores [39]. In a previous work [31] about the hydrocracking of the PS/VGO blend, another deactivation cause at low reaction temperature was identified. In these conditions, the unconverted PS also contributed to catalyst deactivation, since the partially degraded PS molecules deposited on the particles of the catalyst totally blocked its porous structure. Equally, it was verified that an increase in the temperature reduces the significance of this deactivation cause, but increases the importance of the presence of carbonaceous material (internal coke) in the channels of the HY zeolite. The formation of the internal coke lies in the condensation reactions of the aromatics in the reaction medium, which take place in the acidic sites of the zeolite and are boosted at high temperatures [40].

The SEM images of the spent catalysts obtained at the different reaction temperatures (Fig. 2) allow for assessing the incidence of this variable in the relative significance of the different deactivation causes. At 380 °C, the surface of the catalyst presents a smooth envelope that covers almost the totality of the catalyst particles (Fig. 2a). By means of EDX analysis, it has been confirmed that the covering has a carbonaceous nature but is different from the common composition of the catalytic coke. Thus, it can be concluded that this material corresponds to partially degraded PS molecules that have been deposited on the catalyst particles. Furthermore, this problem has not been observed at higher temperatures, exposing that a temperature of 380 °C is not sufficient to propagate the hydrocracking of the PS. Consequently, this particular phenomenon of the hydrocracking of PS must be implemented in the deactivation kinetic, distinguishing it from the deactivation by catalytic coke.

At 400 and 420 °C, the plastic deposition phenomenon is no longer observed since clearer images of the catalyst particles have been obtained (Fig. 2b and c, respectively), and also the drastic catalytic activity decay did not occur [31]. Last, the image displayed in Fig. 2c exposes that heavy metals poisoning (also found at 400 °C) is relevant at 420 °C. This phenomenon has been previously observed in the hydroprocessing of vacuum residue [41]. Indeed, the images show that the highest atomic weight metals do stand out over the low molecular weight species. The brilliant metal particles observed in the spent catalyst (not detected in the fresh catalyst) have been assigned by EDX to Fe and Ni particles, which are found in VGOs [42]. The content of these metals in the deactivated catalysts has been measured by ICP-OES, finding that their content is noticeable and that it follows an increasing trend both with temperature and with time. The highly brilliant particles in Fig. 2d constitute a sort of metal alloy whose formation is possible at 420 °C [43,44]. The formation of these alloys might have a strong influence in catalyst deactivation due to the pores blocked by these deposited metals.

This way, it has been verified that three deactivation causes can be distinguished: (i) fouling caused by the external deposition of PS chains (at low temperature); (ii) internal deposition of catalytic coke; and, (iii) metals poisoning. Hence, three kinetic deactivation equations have been adapted to quantify the deactivation related to each of the causes and their respective expressions have been combined for determining the global deactivation function (ψ in Eq. (1)).

For the deactivation function corresponding to fouling caused by the sedimentation of the partially degraded PS chains (φ_p) the kinetic deactivation model proposed by Elizalde and Ancheyta [45] has been applied. It represented sequentially the coverage of the sites and pores blockage by heavy refractory compounds in the feed by means of two expressions that must be applied before (Eq. (3)) and after (Eq. (4)) the blockage time (t_b):

For $0 < t \leq t_b$.

$$\varphi_p = \varphi_s + (1 - \varphi_s)\, e^{-k_{d,p}t} \tag{3}$$

For $t > t_b$.

$$\varphi_p = \varphi_s + (1 - \varphi_s)\, e^{-k_{d,p}(t - t_b)} \tag{4}$$

where $k_{d,p}$ is the deactivation kinetic constant for plastic deposition and φ_s the steady-state catalyst activity function, in concordance with the consideration made by Monzón et al. [46]. These authors established different deactivation kinetic equations considering that deactivation is usually not complete and that the catalyst achieves a pseudo-stable state with a constant remaining activity.

The deactivation related to the formation of coke has been quantified through a hyperbolic function (Eq. (5)) derived from the Langmuir-Hinshelwood concepts, introducing a constant α, which represents a proportional ratio between the deposited coke on the catalyst (C_c) and the poisoned active sites [23]. The deposited coke on the catalyst was measured in the previous work [31] by means of TG-TPO, whose results are exemplified in Fig. S3 and Table S3, which show TPO profiles and coke contents, respectively. TPO results demonstrate the special increase in the coke amount deposited on the catalysts when coke deposition is the main deactivation route (400 and 420 °C), as well as the displacement on the combustion temperature peak that is related to a higher development of coke structures when temperature is increased.

$$\varphi_c = \frac{1}{(1 + \alpha C_c)^{m_c}} \tag{5}$$

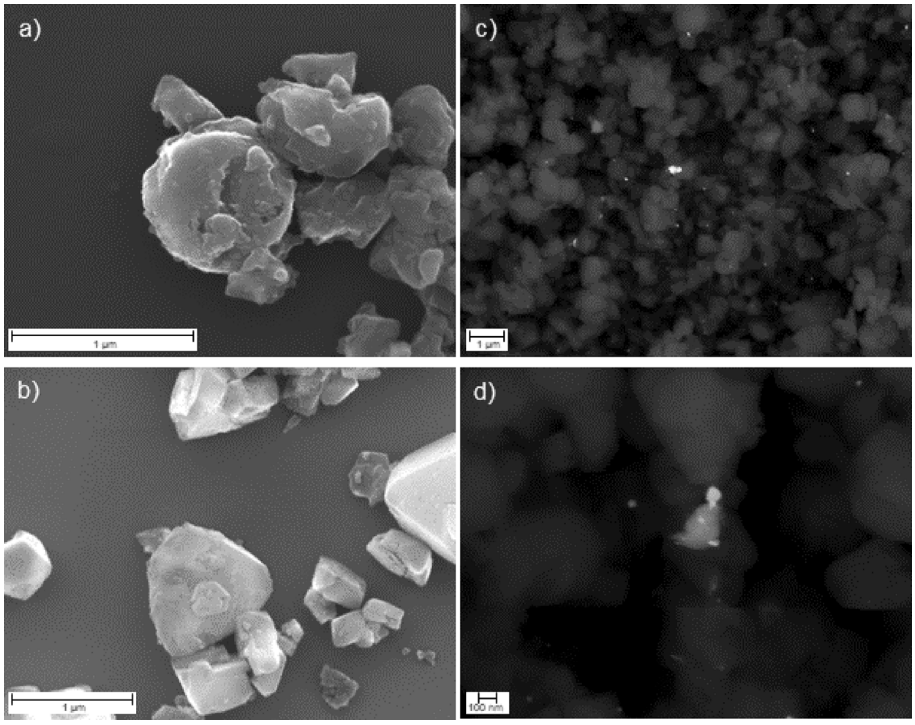

Fig. 2. SEM images of the spent catalysts obtained at 380 °C (a), 400 °C (b) and 420 °C (c and d).

being α the deactivation constant for coke deposition, C_c the carbon fractional content of the catalyst and m_c a fitting parameter (deactivation order by coke).

The equation used for the activity decay related to the metals poisoning is based on an empirical proposal [34] when analyzing the hydrocracking in a slurry reactor. The corresponding deactivation function is dependent on the concentration of the metals in the catalyst (M) and the total metal loading that the catalyst can adsorb (M_0). In this case, the metal loading has been measured from the spent catalysts of the previous work by ICP-AES, as collected on Table S4, which exposes both the trends with time and temperature.

$$\phi_m = 1 - k_{d,m}\left(\frac{M}{M_0}\right)^{m_m} \tag{6}$$

where $k_{d,m}$ is the deactivation kinetic constant for metals poisoning, M is the metal loading for a t time, M_0 is the maximum metal loading that the catalyst can take and m_m is the corresponding deactivation order.

Thus, a global deactivation equation (as defined in Eq. (1)) can be established considering the simultaneous effect of the different causes in the deactivation function [47]. Gayubo et al. [48] consider the synergy between the reversible deactivation (due to coke deposition) and the irreversible one (dealumination) of a HZSM-5 catalyst in methanol conversion to hydrocarbons with the following expression:

$$\psi = \prod_{1}^{n} \varphi_k \tag{7}$$

being n the number of deactivation causes and φ_k the mathematical expression that describes each deactivation cause.

In order to apply Eq. (7) after having analyzed which deactivation causes are involved at each temperature, the catalyst deactivation at 380 °C must be modeled considering the three deactivation causes. Thus, Eqs. (3–5) will be used to quantify the φ_p, φ_c and φ_m deactivation functions, respectively. Equally, following the observations about the deactivation causes involved at 400 and 420 °C, the deactivation function for these temperatures will consider the deposition of coke (φ_c) and the deposition of metallic compounds (φ_m), which are defined by Eqs. (5) and (6), respectively.

3.4. Calculation methodology

The optimization of the apparent values of kinetic constants of the individual reactions, activation energies and deactivation constants established in the kinetic model has been accomplished by adjusting the experimental data of the evolution with the extent of time of the yield of each lump (determined in a previous work [31]) and the predicted values. For that purpose, it has been used an in-house developed MATLAB code that searches for the minimization of the sum of squares of the errors between experimental and predicted values:

$$SSE = \sum_{1}^{n_l}\sum_{1}^{n_d}\left(Y_i^{\exp} - Y_i^{calc}\right)^2 \tag{8}$$

where n_l is the number of lumps in the reaction network, n_d is the number of experimental data, Y_i^{exp} is the experimentally obtained yield and Y_i^{calc} is the corresponding computed yield.

Additionally, the code also calculates the residual values for each parameter, the Jacobian matrix and the correlation coefficient matrix. The mathematical procedure followed for their determination is explained by Amin et al. [49].

The discrimination between the different reaction networks in Fig. 1 has been realized by comparing not only the SSE of the corresponding kinetic models but also performing a significance test based on Fisher's method. For this purpose, the following criterion must be fulfilled [35]:

$$F_{A-B} = \frac{\frac{SSE_A - SSE_B}{SSE_B}}{\frac{\upsilon_A - \upsilon_B}{\upsilon_B}} > F_{1-\alpha}(\upsilon_A - \upsilon_B, \upsilon_B) \tag{9}$$

where υ are the degrees of freedom of each kinetic model, α is considered as 0.05 (that corresponds to a level of significance of 95 %), and $F_{1-\alpha}$ is the critical value for Fisher's distribution and it is calculated by using the function *finv* available in MATLAB software. The basis of this method is that if the inequality of Eq. (14) is fulfilled, then the improvement provided by a kinetic model B with respect to a kinetic model A is significant. This methodology can be applied when two models have different degrees of freedom, which are calculated as follows:

$$\upsilon = n_l n_e - n_p \tag{10}$$

being n_l the number of lumps, n_e the number of experiments and n_p the number of parameters.

4. Results and discussion

4.1. Model discrimination

In order to establish the most appropriate kinetic model, different stages have been followed, comparing the fitting to the experimental data of each of the models described above in Table 1. Firstly, the kinetic models corresponding to the models A and B (explained in Section 3.1 and described in Fig. 1) have been compared. To simplify, it has been considered that the catalyst deactivation is only by coke deposition (main cause of catalyst deactivation at 400 and 420 °C, temperatures of greater interest due to the high conversion of PS achieved). Secondly, after having selected the best reaction network, it has been assessed the interest of considering the three deactivation causes (model B-2). In addition, the possibility of considering the effect of non-catalytic stages occurring in parallel with the catalytic mechanism has been evaluated (model B-3). The statistical parameters calculated in the model discrimination have been collected in Table 1.

In the first stage, which is the comparison of the reaction networks displayed in Fig. 1, model B has been taken as the benchmark because its corresponding kinetic model presents the highest degrees of freedom. Thus, it has been checked if the reduction of the degrees of freedom by applying model A is statistically significant. Attending to the results (Table 1), it can be seen that the SSE obtained with model A has been lower than that of model B (19.35 vs 21.22, respectively), but the criterion detailed in Eq. (9) has not been fulfilled. Therefore, the reaction network proposed in model B remains a better option.

To improve the kinetic model, it has been established the kinetic model B-2 that uses the same reaction network as model B but it considers the three different deactivation causes in the computing of the deactivation function. The degrees of freedom of kinetic model B-2 have been reduced to 62, so kinetic model B has been taken once again as reference for applying the Fisher's test (Eq. (9)). As it can be seen in Table 1, the SSE obtained with kinetic model B-2 is notoriously inferior to that obtained with model B (8.12 vs 21.22, respectively). In addition, the value of F_{B-A} is higher than that of $F_{1-\alpha}$ (16.67 vs 2.25, respectively). Hence, the inclusion of the different deactivation routes, i.e. kinetic model B-2, statistically improves the description made by kinetic model B, with the same reaction network (model B in Fig. 1).

The last proposal (kinetic model B-3) has consisted on including the

Table 1
Statistical comparison between the proposed kinetic models.

Model	Lumps	Deactivation functions	ν	F_{A-B}	$F_{1-\alpha}$	SSE
A	6	1	63	1.22	2.36	19.35
B	7	1	68	–	–	21.22
B-2	7	3	62	16.67	2.25	8.12
B-3	7	3	44	–	1.84	14.76

thermal reaction pathways to Model B-2, by the addition of supplementary first-order reactions for all the individual reactions in the network reaction of model B in Fig. 1, except for the reactions in which the HCO lump is involved, as they have been modeled with second-order reactions. Once again, the results of the fitting have been summarized in Table 1. This time, the SSE obtained with kinetic model B-3 has not improved the results previously obtained with model B-2 in spite of its higher number of kinetic parameters. Therefore, the inclusion of the thermal routes has not improved the fitting.

To sum up, the best results have been obtained with kinetic model B-2, which considers the reaction network of 7-lumps (model B in Fig. 1) and the three different deactivation causes described in Section 3.3. The apparent kinetic constants of this model have been related in Table 2. The subsequent sections will explore the fitting of this model, the predicted values with respect to those experimentally obtained, the evolution of the different activity functions with time, and it will be used to find the optimal operating conditions.

4.2. Fitting and model validation

The optimized parameters corresponding to kinetic model B-2 (Table 2) have been used for calculating the yields of each lump at the three studied temperatures and different reaction times. The comparison between experimental data and the predicted response has been collected in a parity plot displayed in Fig. 3. Overall, a good accuracy of the model has been achieved, even considering the fitting difficulty at 380 °C, when a rapid deactivation occurs because of the blocking of the active sites and porous structure by the deposition of the partially converted PS chains.

This fitting can be observed in more detailing Fig. 4, where the experimental data (symbols) are shown over the predicted data (lines) in different graphs that collect the evolution of the yield of each lump with the time. Apart from the good fit observed on the graphs, two main considerations can be extracted from these graphs. The deviations are mainly attributed to experimental errors in the measure of the yield of PS (unconverted fraction) at 380 °C, as it is a viscous mixture whose evolution with time is difficult to quantify. Thus, the experimental error at 380 °C is noteworthy if the focus is moved to HCO and naphtha yields. On the other side, the fitting of the HCO and DG lumps at 420 °C from 120 min onwards could have been improved by including thermal routes. Indeed, the production of gases through thermal routes in the hydrocracking of hydrocarbon streams has been already observed [18] and even the consideration of these routes has improved the quality of the model [50]. However, as aforementioned (Section 4.1), in this work the inclusion of the thermal routes did not improve the overall fitting of the model.

Table 2
Apparent kinetic parameters at the reference temperature and corresponding apparent activation energies calculated with kinetic model B-2.

Reaction	Parameter	$k_{j,Tref}$	Units	E_j (kJ/mol)
PS → Coke	k_1	(2.47 ± 0.2) 10^{-2}	$g_{cat}^{-1}h^{-1}$	122
PS → LCO	k_2	(3.19 ± 0.3) 10^{-1}	$g_{cat}^{-1}h^{-1}$	49
PS → Naphtha	k_3	(1.01 ± 0.1) 10^{0}	$g_{cat}^{-1}h^{-1}$	224
PS → LPG	k_4	(4.27 ± 0.1) 10^{-2}	$g_{cat}^{-1}h^{-1}$	355
PS → DG	k_5	(5.17 ± 0.4) 10^{-3}	$g_{cat}^{-1}h^{-1}$	413
HCO → Coke	k_6	(4.74 ± 1.0) 10^{-5}	$g_{cat}^{-1}\,g_{HCO}^{-1}h^{-1}$	1
HCO → LCO	k_7	(1.82 ± 0.2) 10^{-2}	$g_{cat}^{-1}\,g_{HCO}^{-1}h^{-1}$	281
HCO → Naphtha	k_8	(1.82 ± 0.1) 10^{-4}	$g_{cat}^{-1}\,g_{HCO}^{-1}h^{-1}$	298
HCO → LPG	k_9	(5.19 ± 0.8) 10^{-5}	$g_{cat}^{-1}\,g_{HCO}^{-1}h^{-1}$	337
HCO → DG	k_{10}	(2.72 ± 0.1) 10^{-5}	$g_{cat}^{-1}\,g_{HCO}^{-1}h^{-1}$	480
LCO → Naphtha	k_{11}	(6.92 ± 0.2) 10^{-1}	$g_{cat}^{-1}h^{-1}$	114
LCO → LPG	k_{12}	(1.45 ± 0.3) 10^{-1}	$g_{cat}^{-1}h^{-1}$	121
LCO → DG	k_{13}	(2.19 ± 0.1) 10^{-2}	$g_{cat}^{-1}h^{-1}$	207
Naphtha → LPG	k_{14}	(9.09 ± 0.5) 10^{-2}	$g_{cat}^{-1}h^{-1}$	43
Naphtha → DG	k_{15}	(8.03 ± 0.3) 10^{-4}	$g_{cat}^{-1}h^{-1}$	65
LPG → DG	k_{16}	(2.34 ± 0.3) 10^{-2}	$g_{cat}^{-1}h^{-1}$	12
Coke → HCO	k_{17}	(6.73 ± 0.5) 10^{-3}	$g_{cat}^{-1}h^{-1}$	1
Plastic fouling	$k_{d,p}$	(4.29 ± 0.3) 10^{-2}	h^{-1}	–
Coke deposition	$\alpha_{d,c}$	(4.69 ± 0.5) 10^{1}	–	–
Metals poisoning	$k_{d,m}$	(3.66 ± 0.1) 10^{-1}	–	188

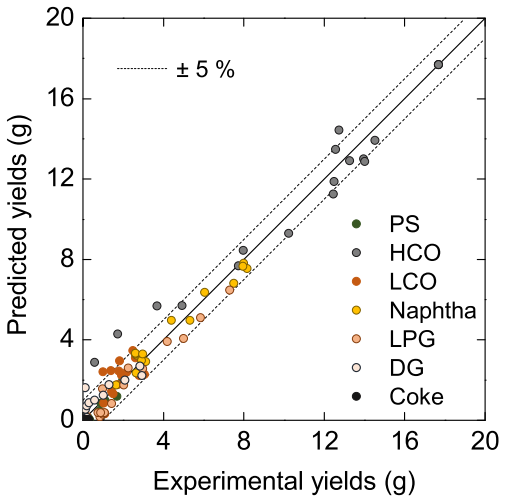

Fig. 3. Parity plot of experimental vs predicted yields with kinetic model B-2 for the different lumps.

4.3. Analysis of kinetic parameters

By comparing the values obtained for the apparent kinetic parameters (Table 2), it can be extracted the importance of the steps in the reaction network (model B in Fig. 1). First, the kinetic parameters of steps #7 and #8 expose the contribution of the HCO lump to the desired products, i.e. LCO and naphtha. The higher value of apparent kinetic constant of step #7 is in agreement with the sequential mechanism established in the literature for the hydrocracking of heavy oils [51]. This mechanism explains that middle distillates are preferentially formed from heavy lumps (HCO), which in turn lead to the formation of lighter species and gases. In the same way, the apparent kinetic parameters in the steps that LCO acts as a reactant (steps #11, #12 and #13) also evidence the primary formation of the naphtha lump.

Concerning naphtha formation, the apparent kinetic constant of steps #2 and #3 allow concluding that the preferred destination of the molecules obtained in the hydrocracking of the PS is the naphtha lump. This fact is consistent with a previous work [13], in which compounds with a boiling range within that of the naphtha fraction were obtained in the hydrocracking of neat PS. Indeed, the formation of not only 1-ring aromatics but also of saturated cyclic compounds was observed.

The reaction network of kinetic model B-2 (Fig. 1b) contemplated the formation of coke from HCO and PS lumps (steps #1 and #6, respectively) because the formation of coke from plastics was previously reported in the literature [52]. Attending to the apparent kinetic constants of these steps it can be observed that this consideration has been appropriate since the kinetic parameters of both steps #1 and #6 are of the same magnitude that other routes of those lumps. However, coke is preferentially formed from HCO lump given the content of 3^{+}-ring aromatics on it (Table S1), although the kinetic parameters cannot be directly compared because of the different order of the reactions. In addition, kinetic model B-2 also contemplates the possibility of coke molecules being converted into HCO molecules (step #17). Even though this step is residual, it has a certain incidence at 420 °C, as the yield of coke goes through a maximum at 120 min (Fig. 4c).

Attending to the values of the apparent activation energy of the formation steps toward the undesirable lump dry gas, the order of these parameters is remarkable: $E_{10} > E_5 > E_{13} > E_{15} > E_{16}$. This highlights the slight effect of temperature on DG formation from the reactants (HCO and PS), as it is the product of the overcracking of primary (LCO,

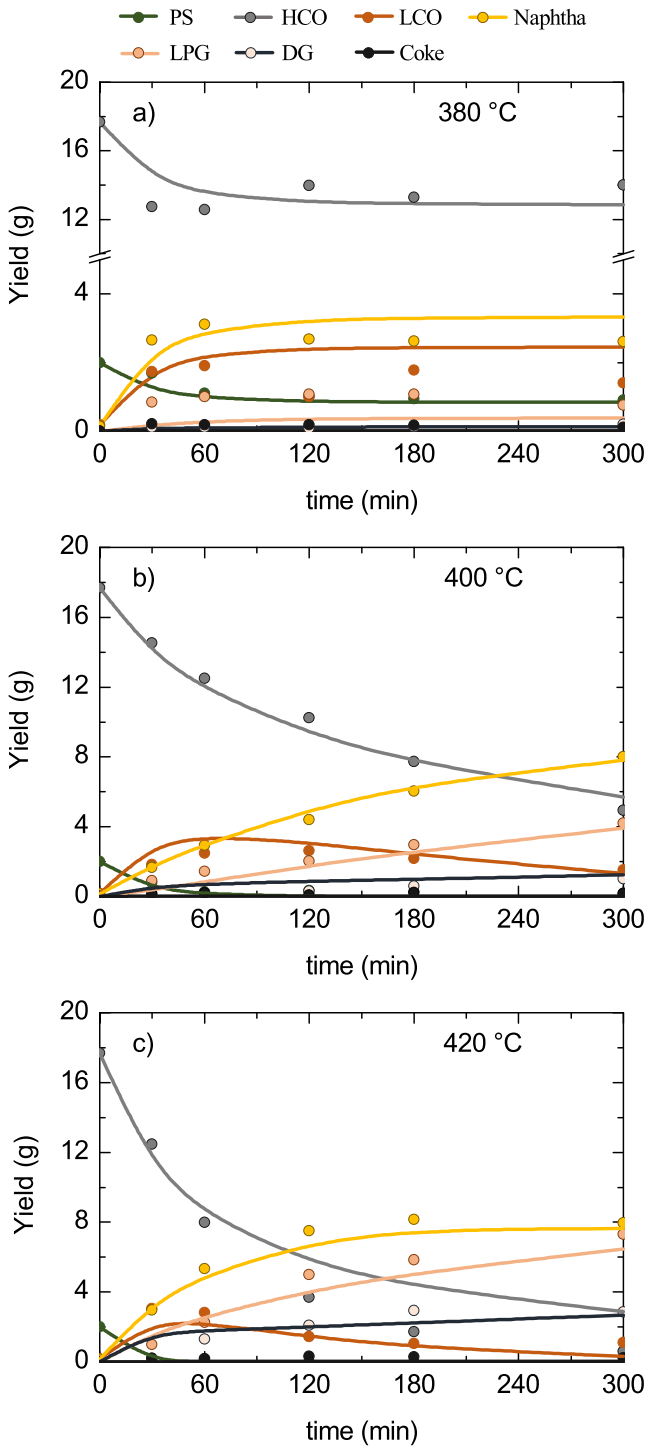

Fig. 4. Fitting of the predicted values (lines) with respect to the experimental yields (scatter).

naphtha) and secondary (LPG) formed lumps.

In order to study the influence and codependence between the kinetic parameters, the correlation matrix of the 17 parameters considered in model B-2 has been obtained (Fig. 5). The matrix depicts the linear association between all the possible pairs of kinetic parameters, allowing discerning between the intrinsic relationships of the proposed mechanism or a strong interrelation due to a bad design of experiments [53]. The values collected in the matrix are within the range –1.0 to 1.0 and the further away the correlation coefficient is from 0, the stronger the linear association between the two kinetic parameters. One should

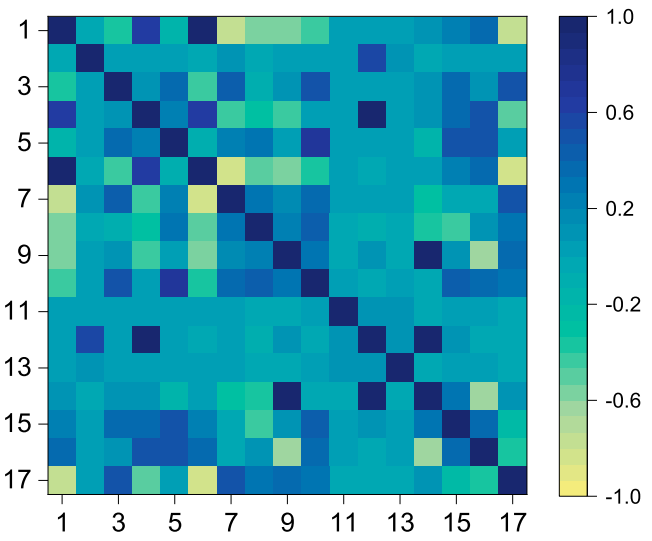

Fig. 5. Coefficient correlation matrix of the kinetic parameters of model B-2.

notice that the correlation matrix is perfectly symmetrical, which means that half of the correlation coefficients shown in the matrix are redundant and unnecessary. Thus the principal diagonal of the matrix is equal to 1.0 because exposes the correlation of each parameter with itself.

This way, strong interdependence between parameters can reveal avoidable steps and therefore modeling parameters, which will help to optimize the number of freedom degrees involved in the model. The interdependence between parameters identify possible over-parametrized routes, as there is a certain degree of uncertainty in the values obtained for those parameters when this correlation is above the critical one [54]. The most noteworthy coefficients are those relating k_4-k_{12}, k_9-k_{14} and k_{12}-k_{14}, all related to the formation of LPG lump. The main reason for this high interrelation can be found in the formation of lumps in a cascade way, as it can be seen on the reaction network in Fig. 1b, the two last parameters connect the formation of LPG from LCO and naphtha, respectively. The formation of naphtha from LCO is precisely one of the most rapid and clear pathways, so the influence of this reaction on LPG formation from both LCO and naphtha is evident. Something similar can be attributed to the interdependence of k_4-k_{12} coefficients, as the PS is mainly converted into LCO and naphtha so the subsequent production of LPG is directly influenced by reaction #4. However, the suppression of any of these paths seems unreasonable as the direct formation of LPG compounds from PS, LCO and naphtha has been proven in literature [55].

4.4. Activity evolution and importance of deactivation causes

The adequate consideration of catalyst deactivation (Section 3.3) has a great impact on kinetic model fitting. Fig. 6 shows the evolution over time of the catalyst activity for the different temperatures of reaction. Continuous lines represent global activity (ψ) and dashed lines describe the deactivation functions related to coke (φ_c) and metal (φ_m) deposition defined in Eqs. (5) and (6), respectively. Deactivation due to PS fouling (φ_p) has not been displayed on Fig. 6 because of being the main deactivation only at 380 °C and at this temperature the global deactivation is almost equal to PS fouling deactivation. At 400 and 420 °C this function value is very close to the unity and therefore it is not shown on in Fig. 6.

Two significant conclusions can be extracted from the activity profiles. First, the activity decay related to plastic deposition at 380 °C is very quick and it is halved in less than 30 min. Moreover, the remaining activity from 120 min and onwards is marginal. In fact, the pore blockage time, defined as one of the optimizing parameters (Eq. (9)), agrees with the experimental observation, resulting in $t_b = 28$ min. Even though coke and metals poisoning have been also considered in the

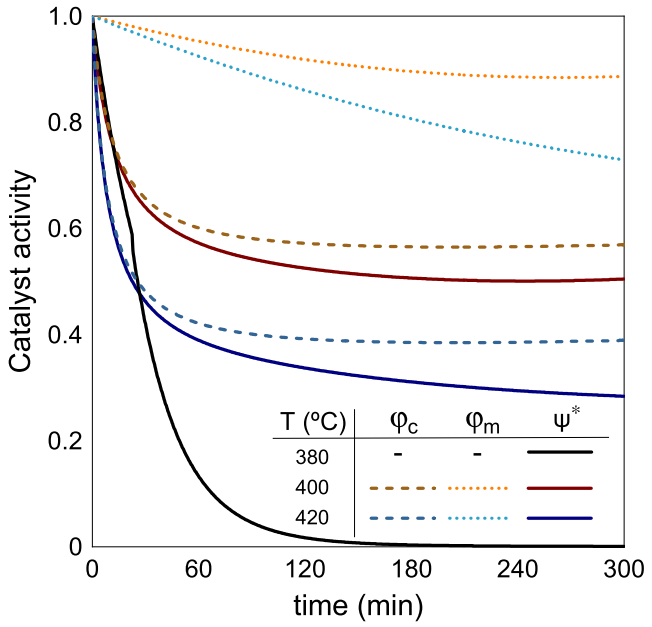

Fig. 6. Evolution of the catalyst activity functions with the reaction time with the separate contribution of deactivation by coke deposition and metals poisoning. ψ^* (380 °C) = φ_p.

kinetic modeling at 380 °C, the PS fouling eclipses their effect and thereby they are not shown in Fig. 6. In contrast, at 400 and 420 °C, when the PS fouling is insignificant because of the evidence discussed in *Section 3.3*, different levels of the catalyst activity prevail after 300 min. Thus, the remaining activity is of 0.50 and 0.28 at 400 and 420 °C, respectively.

On the other hand, the comparison of the deactivation functions evolution due to coke and metals poisoning at 400 and 420 °C confirms the different importance of the two deactivation causes. Although they present considerably different remaining activities, coke deposition is the main cause of deactivation at both temperatures. As for metal deposition, its activity decay doubles its magnitude when increasing temperature from 400 to 420 °C, confirming its strong temperature dependence.

The pseudo-stable remaining activity observed for coke deactivation function at 400 and 420 °C is characteristic of this type of deactivation in hydroprocessing, as the rate of condensation of the coke precursors is compensated by their hydrocracking rate, favored by high hydrogen pressures and the catalyst activity. This situation has been observed in the hydrodeoxygenation of bio-oil [56] and has been considered for the kinetic model of this reaction over an acid activated carbon based bifunctional catalyst [57].

4.5. Operation maps: Optimization

The kinetic model allows performing reactor simulations to find the optimal operating conditions according to the established goals. The simulation has been carried out above 400 °C to avoid the rapid deactivation of the catalyst caused by the unreacted PS chains. In this way, the temperature range used has been 400–440 °C and reaction time has been extended up to 480 min, to obtain a full picture of the framework of the operation. Fig. 7 shows the predicted values over temperature and through reaction time of the yields of PS, naphtha, LPG and DG lumps, as they are the ones with the highest interest to be optimized. The optimization strategy has been established according to different issues that will be relevant when facing the scaling-up of the process (in which a continuous reactor will be used). Thus, plastic conversion should be maximized (by obtaining the minimum yields of PS) in order to prioritize the elimination of the waste plastic and avoid solid deposits from unconverted plastic that would result in operation stops [58]. Moreover, naphtha is a priority in a hydrocracking unit as the production of high-quality gasoline-like streams from alternative feeds is gaining attention due to oil depletion [59]. Last, the extent of the formation of the dry gas by overcracking must be kept under control to maximize selectivity towards naphtha or LCO, which are the products of commercial interest as fuels [60].

Fig. 7a shows that above 400 °C PS yields are less than 1 wt%, which means plastic conversions of 90 %, for times higher than 60 min. The line corresponding to 0.1 wt% yield represents a conversion of a 99 %,

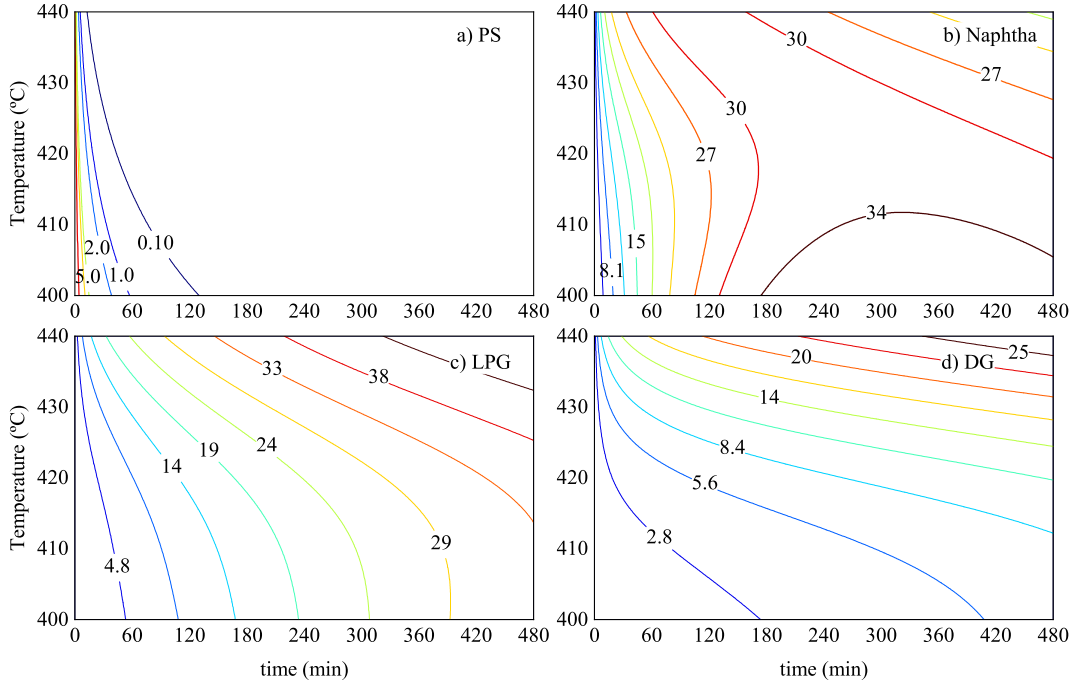

Fig. 7. Prediction with the kinetic model of temperature and reaction time effect on the yields (wt%) of PS (a), naphtha (b), LPG (c) and DG (d) lumps.

demonstrating that almost full conversion can be achieved at 400 °C above 120 min. Besides, at 400 °C and for times higher than 180 min naphtha yield (Fig. 7b) can be maximized with a total yield of 34 wt%. Therefore, the commitment between the yields of naphtha and gases will be critical within the scope of full plastic conversion. Fig. 7c and d evidence the well-known effect of temperature on overcracking reactions, promoting the production of gases when the temperature is risen from 400 °C to above. Taking into account that the maximum yield of naphtha is achieved at 400 °C and for times equal to or greater than 180 min, with full conversion of the plastic and that reaction times and temperatures higher produce higher amounts of lower-value gases (increasing their production in almost a 40 wt% in one hour at 400 °C), optimum conditions must be established at 400 °C and 180 min.

5. Conclusions

The kinetic parameters of a 7-lumps model have been estimated for the joint valorization of PS and VGO in a batch reactor operating at 380–420 °C and with reactions of 30–300 min. Different deactivation causes have been contemplated depending on the reaction temperature. This way, catalyst activity loss can be a consequence of plastic deposition, coke formation and metals poisoning. The application of each deactivation mechanism to the different reaction temperatures has been substantiated by experimental evidence. Moreover, the kinetic model has been used to predict the optimal operating conditions, finding that reactions carried out at 400 °C and for 180 min provide: (i) full conversion of the PS (avoiding at the same time PS fouling as a deactivation cause); (ii) a minimal fraction of the products suffering from overcracking towards gas products; and (iii) a selectivity of naphtha and middle distillates of ca. 50 wt%, with a yield of naphtha of 34 wt%. Coke deposition is the main cause of the catalyst deactivation, but at 400 °C the catalyst activity achieves a pseudo-stable value of the 50 % of the initial one from the 120 min of reaction.

The kinetic model is attractive for the simulation of continuous reactors with the aim of scaling up the process of the hydrocracking of PS and VGO, which is a rational solution for the management of waste plastics. The application of this model to different plastics is now to be applied, with optimistic predictions based on its consideration as an individual lump, in such a way that the kinetic parameters can be recalculated in accordance with each polymer's properties and their synergistic effects with the VGO. Even though the obtained kinetic parameters correspond to the hydrocracking of a PS/VGO (10 wt%) mixture, the methodology here employed can be extended to different compositions and feeds (including different plastics and refinery streams). In addition, the applicability of the model does not only focus on naphtha production but also on targeting different products. Last, the great effect of deactivation in the results encourages deepening in the kinetic modeling of deactivation mechanisms based on the experimental study of the individual incidence of coke and metals deposition on the catalyst activity decay.

Declaration of Competing Interest

The authors declare that they have no known competing financial interests or personal relationships that could have appeared to influence the work reported in this paper.

Data availability

The authors are unable or have chosen not to specify which data has been used.

Acknowledgments

This work has been carried out with the financial support of the Ministry of Science, Innovation and Universities (MICIU) of the Spanish Government (grant RTI2018-096981-B-I00), the European Union's ERDF funds and Horizon 2020 research and innovation program under the Marie Skłodowska-Curie Actions (grant No 823745) and the Basque Government (grant IT1645-22). David Trueba thanks the University of the Basque Country UPV/EHU for his PhD grant (PIF 2018).

The authors thank for technical and human support provided by SGIker of UPV/EHU and European funding (ERDF and ESF). The authors also acknowledge Petronor refinery for providing the feed used in the work.

Appendix A. Supplementary data

Supplementary data to this article can be found online at https://doi.org/10.1016/j.cej.2022.138709.

References

[1] I. Antonopoulos, G. Faraca, D. Tonini, Recycling of post-consumer plastic packaging waste in the EU: recovery rates, material flows, and barriers, Waste Manag 126 (2021) 694–705, https://doi.org/10.1016/j.wasman.2021.04.002.
[2] Z. Yang, F. Lü, H. Zhang, W. Wang, L. Shao, J. Ye, et al., Is incineration the terminator of plastics and microplastics? J. Hazard. Mater. 401 (2021), 123429 https://doi.org/10.1016/j.jhazmat.2020.123429.
[3] A. Xu, M. Shi, X. Xing, Y. Su, X. Li, W. Liu, et al., Status and prospects of atmospheric microplastics: a review of methods, occurrence, composition, source and health risks, Environ. Pollut. 303 (2022), 119173, https://doi.org/10.1016/j.envpol.2022.119173.
[4] R.-X. Yang, K. Jan, C. Chen, W.-T. Chen, K.-C.-W. Wu, Thermochemical conversion of plastic waste into fuels, chemicals, and value-added materials: a critical review and outlooks, ChemSusChem (2022) e202200171, https://doi.org/10.1002/cssc.202200171.
[5] F. Zhang, F. Wang, X. Wei, Y. Yang, S. Xu, D. Deng, et al., From trash to treasure: chemical recycling and upcycling of commodity plastic waste to fuels, high-valued chemicals and advanced materials, J. Energy Chem. 69 (2022) 369–388, https://doi.org/10.1016/j.jechem.2021.12.052.
[6] R. Palos, A. Gutiérrez, F.J. Vela, M. Olazar, J.M. Arandes, J. Bilbao, Waste Refinery: the valorization of waste plastics and end-of-life tires in refinery units. A review, Energy and Fuels 35 (2021) 3529–3557, https://doi.org/10.1021/acs.energyfuels.0c03918.
[7] G. Lopez, M. Artetxe, M. Amutio, J. Bilbao, M. Olazar, Thermochemical routes for the valorization of waste polyolefinic plastics to produce fuels and chemicals. A review, Renew. Sustain Energy Rev. 73 (2017) 346–368, https://doi.org/10.1016/j.rser.2017.01.142.
[8] Osman AI, Farrell C, Al-Muhtaseb AH, Al-Fatesh AS, Harrison J, Rooney DW. Pyrolysis kinetic modelling of abundant plastic waste (PET) and in-situ emission monitoring n.d. 10.1186/s12302-020-00390-x.
[9] G. Lopez, M. Artetxe, M. Amutio, J. Alvarez, J. Bilbao, M. Olazar, Recent advances in the gasification of waste plastics. A critical overview, Renew. Sustain. Energy Rev. 82 (2018) 576–596, https://doi.org/10.1016/j.rser.2017.09.032.
[10] E. Rodríguez, A. Gutiérrez, R. Palos, F.J. Vela, M.J. Azkoiti, J.M. Arandes, et al., Co-cracking of high-density polyethylene (HDPE) and vacuum gasoil (VGO) under refinery conditions, Chem. Eng. J. 382 (2020), https://doi.org/10.1016/j.cej.2019.122602.
[11] E. Rodríguez, R. Palos, A. Gutiérrez, D. Trueba, J.M. Arandes, J. Bilbao, Towards waste refinery: Co-feeding HDPE pyrolysis waxes with VGO into the catalytic cracking unit, Energy Convers Manag. 207 (2020), 112554, https://doi.org/10.1016/j.enconman.2020.112554.
[12] R. Palos, E. Rodríguez, A. Gutiérrez, J. Bilbao, J.M. Arandes, Cracking of plastic pyrolysis oil over FCC equilibrium catalysts to produce fuels: kinetic modeling, Fuel 316 (2022), 123341, https://doi.org/10.1016/j.fuel.2022.123341.
[13] D. Munir, M.F. Irfan, M.R. Usman, Hydrocracking of virgin and waste plastics: A detailed review, Renew. Sustain. Energy Rev. 90 (2018) 490–515, https://doi.org/10.1016/j.rser.2018.03.034.
[14] V.L. Mangesh, P. Tamizhdurai, P. Santhana Krishnan, S. Narayanan, S. Umasankar, S. Padmanabhan, et al., Green energy: Hydroprocessing waste polypropylene to produce transport fuel, J Clean Prod 276 (2020), 124200, https://doi.org/10.1016/j.jclepro.2020.124200.
[15] B.C. Vance, P.A. Kots, C. Wang, Z.R. Hinton, C.M. Quinn, T.H. Epps, et al., Single pot catalyst strategy to branched products via adhesive isomerization and hydrocracking of polyethylene over platinum tungstated zirconia, Appl. Catal. B Environ. 299 (2021), 120483, https://doi.org/10.1016/j.apcatb.2021.120483.
[16] I.-H. Choi, H.-J. Lee, G.-B. Rhim, D.-H. Chun, K.-H. Lee, K.-R. Hwang, Catalytic hydrocracking of heavy wax from pyrolysis of plastic wastes using Pd/Hβ for naphtha-ranged hydrocarbon production, J. Anal. Appl. Pyrol. 161 (2022), 105424, https://doi.org/10.1016/j.jaap.2021.105424.
[17] J.W. Thybaut, G.B. Marin, Multiscale aspects in hydrocracking: from reaction mechanism over catalysts to kinetics and industrial application, Adv. Catal. 59 (2016) 109–238, https://doi.org/10.1016/bs.acat.2016.10.001.
[18] F.J. Vela, R. Palos, J. Bilbao, J.M. Arandes, A. Gutiérrez, Effect of co-feeding HDPE on the product distribution in the hydrocracking of VGO, Catal. Today 353 (2020) 197–203, https://doi.org/10.1016/j.cattod.2019.07.010.

[19] F.J. Vela, R. Palos, D. Trueba, J. Bilbao, J.M. Arandes, A. Gutiérrez, Different approaches to convert waste polyolefins into automotive fuels via hydrocracking with a NiW/HY catalyst, Fuel Process. Technol. 220 (2021), 106891, https://doi.org/10.1016/j.fuproc.2021.106891.
[20] C.I. Akor, A.I. Osman, C. Farrell, C.S. McCallum, W. John Doran, K. Morgan, et al., Thermokinetic study of residual solid digestate from anaerobic digestion, Chem. Eng. J. 406 (2021), 127039, https://doi.org/10.1016/J.CEJ.2020.127039.
[21] A. Quitian, J. Ancheyta, Experimental methods for developing kinetic-models for hydrocracking reactions with slurry-phase catalyst using batch reactors, Energy Fuels 30 (2016) 4419–4437, https://doi.org/10.1021/acs.energyfuels.5b01953.
[22] P.J. Becker, N. Serrand, B. Celse, D. Guillaume, H. Dulot, Comparing hydrocracking models: continuous lumping vs. single events, Fuel 165 (2016) 306–315, https://doi.org/10.1016/j.fuel.2015.09.091.
[23] E. Rodríguez, G. Félix, J. Ancheyta, F. Trejo, Modeling of hydrotreating catalyst deactivation for heavy oil hydrocarbons, Fuel 225 (2018) 118–133, https://doi.org/10.1016/j.fuel.2018.02.085.
[24] Z. Till, T. Varga, L. Szabó, T. Chován, Identification and observability of lumped kinetic models for vacuum gas oil hydrocracking, Energy Fuels 31 (2017) 12654–12664, https://doi.org/10.1021/acs.energyfuels.7b02040.
[25] Z. Till, T. Varga, J. Sója, N. Miskolczi, T. Chován, Reduction of lumped reaction networks based on global sensitivity analysis, Chem. Eng. J. 375 (2019), https://doi.org/10.1016/j.cej.2019.121920.
[26] B. Browning, P. Alvarez, T. Jansen, M. Lacroix, C. Geantet, M. Tayakout-Fayolle, A review of thermal cracking, hydrocracking, and slurry phase hydroconversion kinetic parameters in lumped models for upgrading heavy oils, Energy Fuels 35 (2021) 15360–15380, https://doi.org/10.1021/acs.energyfuels.1c02214.
[27] G. Félix, J. Ancheyta, Comparison of hydrocracking kinetic models based on SARA fractions obtained in slurry-phase reactor, Fuel 241 (2019) 495–505, https://doi.org/10.1016/j.fuel.2018.11.153.
[28] A. Bin Jumah, M. Malekshahian, A.A. Tedstone, A.A. Garforth, Kinetic modeling of hydrocracking of low-density polyethylene in a batch reactor, ACS Sustain Chem. Eng. 9 (2021) 16757–16769, https://doi.org/10.1021/acssuschemeng.1c06231.
[29] G. Félix, J. Ancheyta, Using separate kinetic models to predict liquid, gas, and coke yields in heavy oil hydrocracking, Ind. Eng. Chem. Res. 58 (2019) 7973–7979, https://doi.org/10.1021/acs.iecr.9b00904.
[30] L. Han, X. Fang, C. Peng, T. Zhao, Application of discrete lumped kinetic modeling on vacuum gas oil hydrocracking, China Pet Process Petrochemical. Technol. 15 (2013) 67–73.
[31] D. Trueba, R. Palos, J. Bilbao, J.M. Arandes, A. Gutiérrez, Product composition and coke deposition in the hydrocracking of polystyrene blended with vacuum gasoil, Fuel Process. Technol. 224 (2021), 107010, https://doi.org/10.1016/j.fuproc.2021.107010.
[32] R. Palos, A. Gutiérrez, J.M. Arandes, J. Bilbao, Upgrading of high-density polyethylene and light cycle oil mixtures to fuels via hydroprocessing, Catal. Today 305 (2018) 212–219, https://doi.org/10.1016/j.cattod.2017.06.033.
[33] T. Wang, M. Chen, X. Liu, Z.G. Zhang, Y. Xu, Distinguishing external and internal coke depositions on micron-sized HZSM-5: Via catalyst-assisted temperature-programmed oxidation, New J. Chem. 43 (2019) 13938–13946, https://doi.org/10.1039/c9nj02899d.
[34] J. Martínez, J. Ancheyta, Kinetic model for hydrocracking of heavy oil in a CSTR involving short term catalyst deactivation, Fuel 100 (2012) 193–199, https://doi.org/10.1016/j.fuel.2012.05.032.
[35] T. Cordero-Lanzac, A.T. Aguayo, A.G. Gayubo, P. Castaño, J. Bilbao, Simultaneous modeling of the kinetics for n-pentane cracking and the deactivation of a HZSM-5 based catalyst, Chem. Eng. J. 331 (2018) 818–830, https://doi.org/10.1016/j.cej.2017.08.106.
[36] C.J. Calderón, J. Ancheyta, Modeling of CSTR and SPR small-scale isothermal reactors for heavy oil hydrocracking and hydrotreating, Fuel 216 (2018) 852–860, https://doi.org/10.1016/j.fuel.2017.11.089.
[37] S. Sánchez, J. Ancheyta, Effect of pressure on the kinetics of moderate hydrocracking of Maya crude oil, Energy Fuels 21 (2007) 653–661, https://doi.org/10.1021/ef060525y.
[38] M. Schwaab, J.C. Pinto, Optimum reference temperature for reparameterization of the Arrhenius equation. Part 1: problems involving one kinetic constant, Chem. Eng. Sci. 62 (2007) 2750–2764, https://doi.org/10.1016/j.ces.2007.02.020.
[39] T. Cordero-Lanzac, I. Hita, A. Veloso, J.M. Arandes, J. Rodríguez-Mirasol, J. Bilbao, et al., Characterization and controlled combustion of carbonaceous deactivating species deposited on an activated carbon-based catalyst, Chem. Eng. J. 327 (2017) 454–464, https://doi.org/10.1016/J.CEJ.2017.06.077.
[40] A. Gutiérrez, J.M. Arandes, P. Castaño, A.T. Aguayo, J. Bilbao, Role of acidity in the deactivation and steady hydroconversion of light cycle oil on noble metal supported catalysts, Energy Fuels 25 (2011) 3389–3399, https://doi.org/10.1021/ef200523g.
[41] P. Torres-Mancera, J. Ancheyta, J. Martínez, Deactivation of a hydrotreating catalyst in a bench-scale continuous stirred tank reactor at different operating conditions, Fuel 234 (2018) 326–334, https://doi.org/10.1016/j.fuel.2018.06.122.
[42] E. Rodríguez, R. Palos, A. Gutiérrez, J.M. Arandes, J. Bilbao, Scrap tires pyrolysis oil as a co-feeding stream on the catalytic cracking of vacuum gasoil under fluid catalytic cracking conditions, Waste Manag 105 (2020) 18–26, https://doi.org/10.1016/j.wasman.2020.01.026.
[43] L. Li, S. Zuo, P. An, H. Wu, F. Hou, G. Li, et al., Hydrogen production via steam reforming of n-dodecane over NiPt alloy catalysts, Fuel 262 (2020), 116469, https://doi.org/10.1016/J.FUEL.2019.116469.
[44] J. Zhang, X. Hu, B. Yang, N. Su, H. Huang, J. Cheng, et al., Novel synthesis of PtPd nanoparticles with good electrocatalytic activity and durability, J. Alloy. Compd. 709 (2017) 588–595, https://doi.org/10.1016/J.JALLCOM.2017.03.202.
[45] I. Elizalde, J. Ancheyta, Modeling catalyst deactivation during hydrocracking of atmospheric residue by using the continuous kinetic lumping model, Fuel Process. Technol. 123 (2014) 114–121, https://doi.org/10.1016/j.fuproc.2014.02.006.
[46] A. Monzón, E. Romeo, A. Borgna, Relationship between the kinetic parameters of different catalyst deactivation models, Chem. Eng. J. 94 (2003) 19–28, https://doi.org/10.1016/S1385-8947(03)00002-0.
[47] J. Corella, A. Monzón, Modeling of the deactivation kinetics of solid catalysts by two or more simultaneous and different causes, Ind. Eng. Chem. Res. 27 (1988) 369–374, https://doi.org/10.1021/ie00075a001.
[48] A.G. Gayubo, A.T. Aguayo, M. Olazar, R. Vivanco, J. Bilbao, Kinetics of the irreversible deactivation of the HZSM-5 catalyst in the MTO process, Chem. Eng. Sci. 58 (2003) 5239–5249, https://doi.org/10.1016/J.CES.2003.08.020.
[49] S.S. Amin, H. Abdollahi, A. Naseri, The influence of coupled kinetic-equilibrium in breaking the correlation between kinetic parameters, Chemom. Intell. Lab. Syst. 215 (2021), 104349, https://doi.org/10.1016/j.chemolab.2021.104349.
[50] H.H. Pham, N. Thuy Nguyen, K.S. Go, S. Park, N. Sun Nho, G.T. Kim, et al., Kinetic study of thermal and catalytic hydrocracking of asphaltene, Catal. Today 353 (2020) 112–118, https://doi.org/10.1016/j.cattod.2019.08.031.
[51] H.H. Pham, K.H. Kim, K.S. Go, N.S. Nho, W. Kim, E.H. Kwon, et al., Hydrocracking and hydrotreating reaction kinetics of heavy oil in CSTR using a dispersed catalyst, J. Pet Sci. Eng. 197 (2021), 107997, https://doi.org/10.1016/j.petrol.2020.107997.
[52] S. Liu, P.A. Kots, B.C. Vance, A. Danielson, D.G. Vlachos, Plastic waste to fuels by hydrocracking at mild conditions, Sci. Adv. 7 (2021) eabf8283, https://doi.org/10.1126/sciadv.abf8283.
[53] G. Schultz, R. Alexander, F.V. Lima, R.C. Giordano, M.P.A. Ribeiro, Kinetic modeling of the enzymatic synthesis of galacto-oligosaccharides: Describing galactobiose formation, Food Bioprod. Process. 127 (2021) 1–13, https://doi.org/10.1016/j.fbp.2021.02.004.
[54] F. Ketzer, F. de Castilhos, An assessment on kinetic modeling of esterification reaction from oleic acid and methyl acetate over USY zeolite, Microporous Mesoporous Mater. 314 (2021), 110890, https://doi.org/10.1016/j.micromeso.2021.110890.
[55] A. Bin Jumah, A.A. Tedstone, A.A. Garforth, Hydrocracking of virgin and post-consumer polymers, Microporous Mesoporous Mater. 315 (2021), 110912, https://doi.org/10.1016/j.micromeso.2021.110912.
[56] T. Cordero-Lanzac, R. Palos, J.M. Arandes, P. Castaño, J. Rodríguez-Mirasol, T. Cordero, et al., Stability of an acid activated carbon based bifunctional catalyst for the raw bio-oil hydrodeoxygenation, Appl. Catal. B Environ. 203 (2017) 389–399, https://doi.org/10.1016/j.apcatb.2016.10.018.
[57] T. Cordero-Lanzac, I. Hita, F.J. García-Mateos, P. Castaño, J. Rodríguez-Mirasol, T. Cordero, et al., Adaptable kinetic model for the transient and pseudo-steady states in the hydrodeoxygenation of raw bio-oil, Chem. Eng. J. 400 (2020), 124679, https://doi.org/10.1016/j.cej.2020.124679.
[58] O. Dogu, M. Pelucchi, R. Van de Vijver, P.H.M. Van Steenberge, D.R. D'hooge, A. Cuoci, et al., The chemistry of chemical recycling of solid plastic waste via pyrolysis and gasification: State-of-the-art, challenges, and future directions, Prog. Energy Combust. Sci. 84 (2021), 100901, https://doi.org/10.1016/J.PECS.2020.100901.
[59] M.S. El-Sawy, S.A. Hanafi, F. Ashour, T.M. Aboul-Fotouh, Co-hydroprocessing and hydrocracking of alternative feed mixture (vacuum gas oil/waste lubricating oil/waste cooking oil) with the aim of producing high quality fuels, Fuel 269 (2020), 117437, https://doi.org/10.1016/j.fuel.2020.117437.
[60] Z. Cao, X. Zhang, C. Xu, X. Huang, Z. Wu, C. Peng, et al., Selective hydrocracking of light cycle oil into high-octane gasoline over bi-functional catalysts, J. Energy Chem. 52 (2021) 41–50, https://doi.org/10.1016/j.jechem.2020.04.055.